Shape evolution of electrodeposited bumps into deep cavities

K Hayashi
Okayama University

Keisuke Fukui
Himeji Institute of Technology

Zenzo Tanaka
Okayama University

Kazuo Kondo
Okayama University

Journal of The Electrochemical Society, **148** (3) C145-C148 (2001)
0013-4651/2001/148(3)/C145/4/$7.00 © The Electrochemical Society, Inc.

Shape Evolution of Electrodeposited Bumps into Deep Cavities

K. Hayashi,[a] K. Fukui,[b] Z. Tanaka,[a] and K. Kondo[a,*,z]

[a]*Department of Applied Chemistry, University of Okayama, Okayama 700-0082, Japan*
[b]*Department of Chemical Engineering, Himeji Institute of Technology, Himeji 671-2201, Japan*

Metal posts and finer pitch solder bumps are the indispensable microconnectors for chip size packaging and are formed by electrodeposition into deep cavities. It is difficult to stir inside these deep cavities. Natural convection due to density difference is effective in stirring inside cavity with 200 μm cathode width of aspect ratio of one. The bump shape increases toward lower side in a vertical cathode arrangement with placement angle of $\Theta = 90°$. This increase in bump height results from a collision of flow along the lower side of the resist sidewall which enlarges local current and thickens the lower edge of bumps. The effect of natural convection is also evident in the neighboring two cavities of 200 μm cathode width. The natural convection is not effective for cavities with less than 100 μm cathode width. The bump shapes become flat. Only diffusion occurs within these smaller than 100 μm cavities.
 [DOI: 10.1149/1.1346602]

Manuscript submitted January 19, 2000; revised manuscript received August 28, 2000.

In addition to high integration of chips and compactness of packaging, the miniaturization and high speed improvement of electronics devices can be achieved by high pin count interconnection of chips. Chip size packaging (CSP) and ball grid arrays (BGA) are indispensable for high pin count interconnection. Wafer level CSP is a most promising interconnection technology and the copper bump (metal post) is used as a stress releasing material to accommodate the difference in thermal expansion coefficients between silicon and the printed circuit board. These copper bumps and also finer pitch solder bumps are electrodeposited into deep cavities of more than 1.0 aspect ratio.

The current distribution problems for bumping are extensively discussed by several authors. Dukovic developed a two-dimensional numerical computation of tertiary current distribution only including the diffusion. The moving boundary problem was discussed on shape evolution of copper electrodeposit and the effect of resist wall angle and leveling agent was reported.[1] Leyerdecker *et al.* discussed the importance of diffusion for large aspect ratio cavity of LIGA process.[2] The experimental studies on shape evolution of gold bumps were discussed by Kondo *et al.*[3] The effect of dot diameter, electrolyte flow, and additives on bump shapes was examined. Numerical fluid dynamics computations were performed on the initial stage of gold and copper bump at Peclet numbers less than 100.[4,5] Similarly, computations of copper deposition at Peclet numbers greater than 100 were also reported.[6] The influence of photoresist angles on shape evolution during copper plating has also been described.[7]

The role of convection and diffusion within the deep cavities has also been studied.[8] We found that convection outside the cavity is not effective in stirring the fluid inside deep cavities. No penetration flows and only recirculating vortices form within the deep cavities. Within deeper cavities, the mass transport is controlled mainly by diffusion. For Peclet numbers larger than one, these vortices recirculate within themselves and might represent the mass-transfer resistance between outside cavities and cathodes at cavity bottoms.[6] Hence, we studied the importance of natural convection to stir inside a deep cavity of more than one aspect ratio.[9]

The existence of natural convection is confirmed not only by bump shape observations but also by numerical fluid dynamics computation of 200 μm cathode width cavity. Cavities less than 200 μm in cathode width are discussed.

Experimental

A 200 μm wide cavity was drilled into the acrylic resin plate 200 μm thick. The acrylic resin plate and a copper foil were glued together. The acrylic resin plate is called the resist. Less than 100 μm wide cavities were patterned on photoresist of THB-430N (JSR Co.). The photomask pattern has linewidths of 100, 50, 30, 20, and 10 μm.

The copper foil at the bottom of cavities was used as the cathode and a copper plate anode was implemented along with a 3.33 mol KCl-AgCl reference electrode.

The electrolyte was prepared with 0.60×10^3 mol/m^3 of $CuSO_4$ and 1.856×10^3 mol/m^3 of H_2SO_4. Bumps were formed potentiostatically in the mass-transfer controlled region. The total charge coulomb was adjusted, so that the bump heights were about one-third of the resist heights. Cathode placement angles (Θ) were 0 and 90° with respect to horizontal axis. Bump cross sections were observed by an optical microscope.

Velocity profiles and isoconcentration contours and current distributions were analyzed with two-dimensional numerical fluid dynamics computation. Equation of continuity, Navier-Stokes equations including gravity and mass-transfer equation are given as follows

$$\frac{\partial \rho u}{\partial x} + \frac{\partial \rho v}{\partial y} = 0 \quad [1]$$

$$\rho\left(u\frac{\partial u}{\partial x} + v\frac{\partial u}{\partial y}\right) = -\frac{\partial P}{\partial x} + \mu\left(\frac{\partial^2 u}{\partial x^2} + \frac{\partial^2 u}{\partial y^2}\right) \quad [2]$$

$$\rho\left(u\frac{\partial v}{\partial x} + v\frac{\partial v}{\partial y}\right) = -\frac{\partial P}{\partial y} + \mu\left(\frac{\partial^2 v}{\partial x^2} + \frac{\partial^2 v}{\partial y^2}\right) + \rho g \beta_c (c - c_0) \quad [3]$$

$$\frac{\partial \rho c}{\partial t} + \frac{\partial \rho c u}{\partial x} + \frac{\partial \rho c v}{\partial y} = \frac{\partial}{\partial x}\left(\rho D \frac{\partial c}{\partial x}\right) + \frac{\partial}{\partial y}\left(\rho D \frac{\partial c}{\partial y}\right) \quad [4]$$

The properties of $CuSO_4/H_2SO_4$ solution are given as follows. $\rho = 1.108\text{-}1.196 \times 10^3$ kg/m^3, $c_{bulk} = 0.6 \times 10^3$ mol/m^3, $D = 4.5 \times 10^{-10}$ m^2/s, $\nu = 1.394 \times 10^{-6}$ m^2/s.

Results and Discussion

Bump shapes for 200 μm cavity.—Figure 1 shows the cross section of bumps electrodeposited potentiostatically at the diffusion control region of −110 mV *vs.* 3.33 mol/L KCl-AgCl. Cathode placement angles are also illustrated. The cathode placement angles (Θ) are 90 and 0° for a and c, respectively. The cavity has 200 μm resist height and 200 μm cathode width.

In Fig. 1a, the bump height increases toward right or lower side with cathode placement angle of $\Theta = 90°$. For Fig. 1c of $\Theta = 0°$, the bump is almost flat with a small hump existing at the center of the cross section.

Figure 2 shows the cross section of two neighboring bumps elec-

* Electrochemical Society Active Member.
z E-mail: kkondo@cc.okayama-u.ac.jp

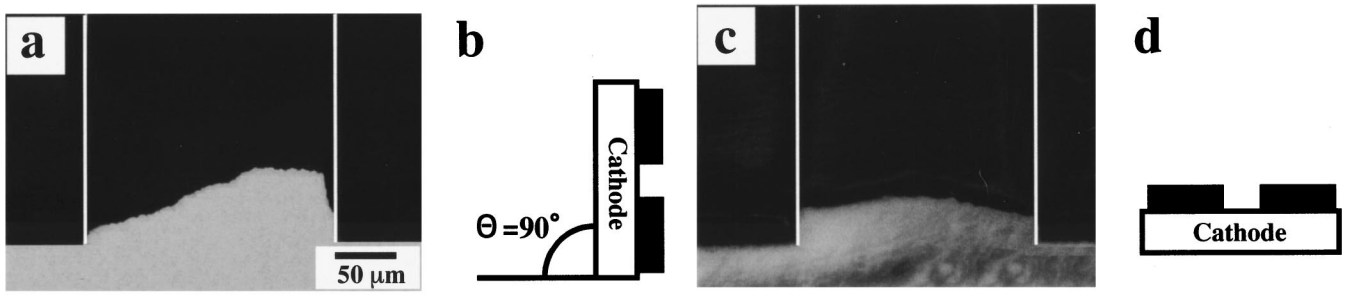

Figure 1. Cross section of bumps with different placement angles (Θ). Cathode width is 200 μm and resist height is 200 μm. (a) θ = 90°, (c) θ = 0°, (b, d) cathode placement illustrating. *x*: horizontal axis, *y*: vertical axis.

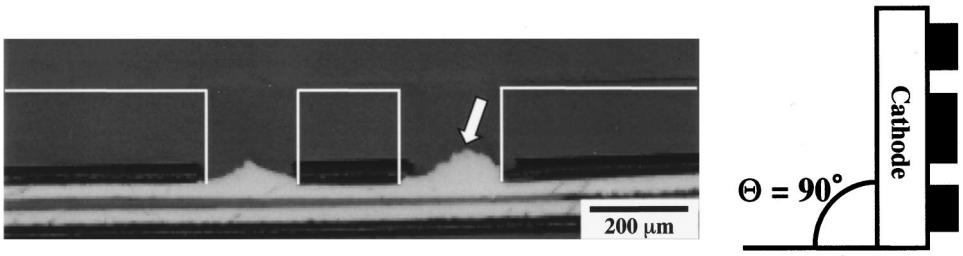

Figure 2. Cross section of bumps with the neighboring 200 μm cavities. Cathode placement angle is 90°.

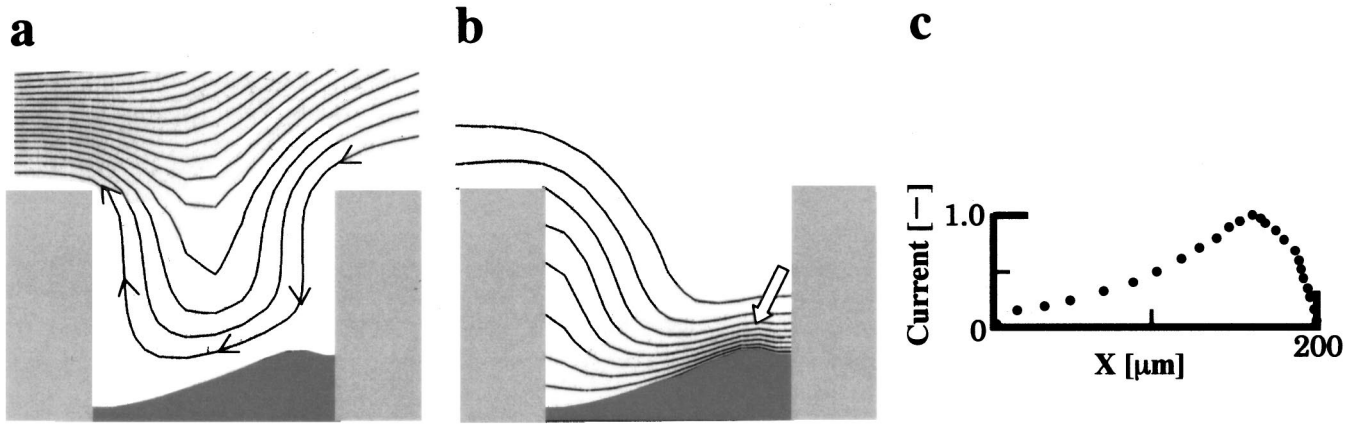

Figure 3. (a) Flow pattern, (b) isoconcentration contour, and (c) current distribution of the cavity of 200 μm resist height and 200 μm cathode width of Θ = 90°.

trodeposited potentiostatically in the diffusion control region. The cathode placement angle is Θ = 90°. The neighboring cavities were separated by 200 μm and have 200 μm resist height and width.

The heights of bumps are different. The right side bump is higher than the left side (indicated with an arrow). The right side again is the lower side of cathode with cathode placement angle of Θ = 90°.

Numerical computation for 200 μm cavity.—Figure 3 shows the flow pattern, isoconcentration contour, and current distribution in a cavity with 200 μm resist height and cathode width of Θ = 90°. A flow from the upper right side of the resist flows downward along the right resist sidewall and collides with the right edge of the bump (Fig. 3a).

Figure 3b shows the isoconcentration contour within the cavity. The neighboring isoconcentration contours are close at the right edge of the cavity. This indicates an increase in mass transport of cupric ion. Since the current is proportional to the mass transport in the diffusion control region, the current shows a maximum value at the right edge of the cavity. This is illustrated in Fig. 3c of the current distribution.

Numerical computation for neighboring 200 μm cavities.—Figure 4 shows the effect of neighboring cavities on the flow patterns, isoconcentration contours, and current distributions. A flow from the right side penetrates into the 200 μm cavities (Fig. 4a). Figure 4b shows the isoconcentration contours. The isoconcentration contours are closer at the right side cavity compared to the left side cavity (indicated with an arrow). This closeness indicates larger mass transport of cupric ion at the right side. Figure 4c is the current distribution. The current at the right side becomes larger if compared to that at the left side which corresponds to the bump heights difference in Fig. 2 (indicated with an arrow).

The natural convection due to density difference is the origin of this mass transport both for a single 200 μm cavity and neighboring 200 μm cavities with cathode placement angle of Θ = 90°. Close to the cathode, cupric ion concentration decreases because of its consumption at the cathode. This decrease in concentration leads to

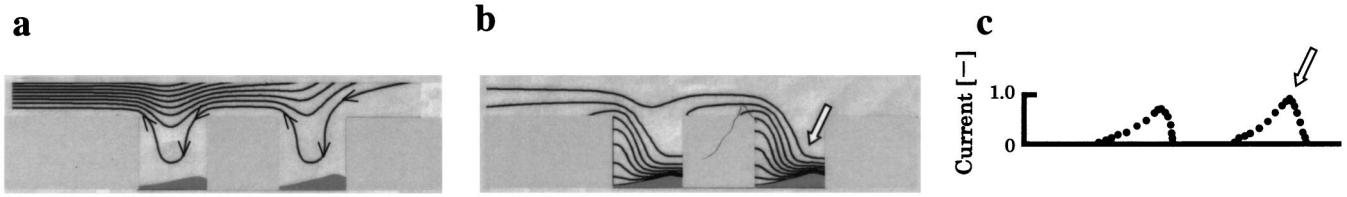

Figure 4. (a) Flow pattern, (b) isoconcentration contour, and (c) current distribution for the neighboring 200 μm cavities.

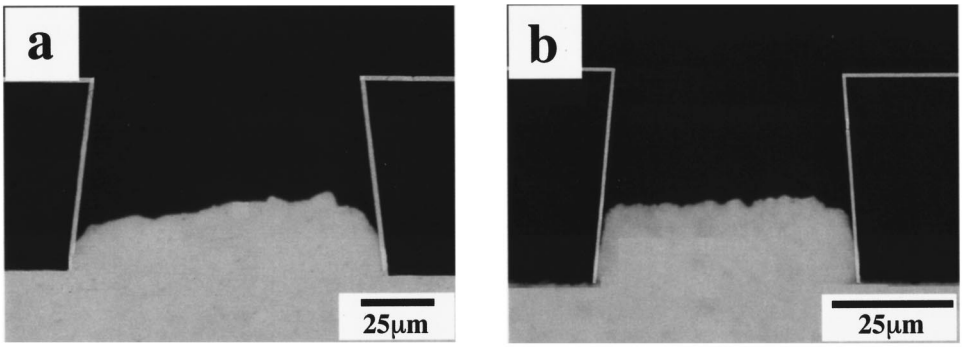

Figure 5. Cross section of bumps with different cathode widths; (a) 100 and (b) 50 μm.

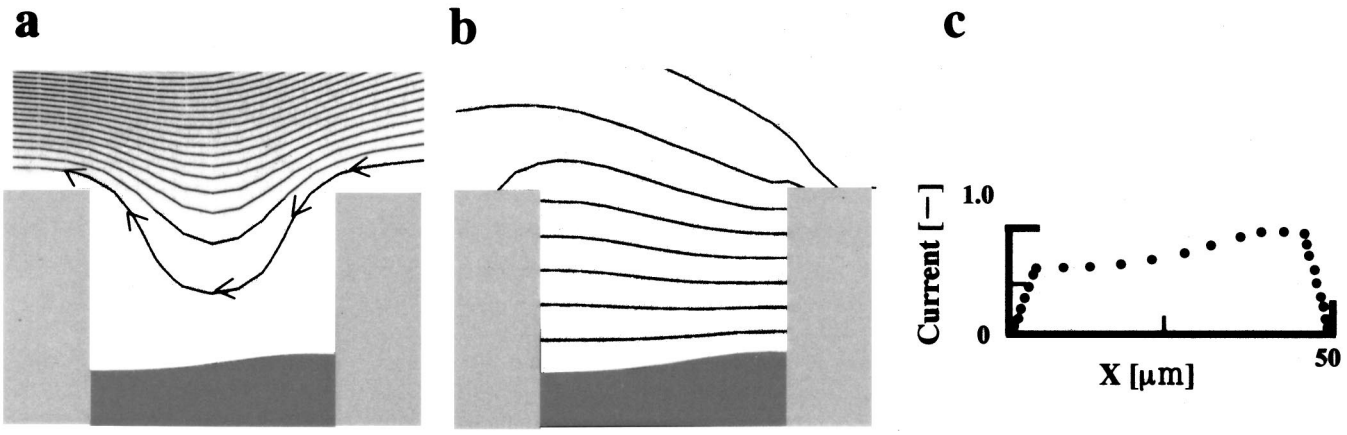

Figure 6. (a) Flow pattern, (b) isoconcentration contour, and (c) current distribution of the cavity of 50 μm cathode width of $\Theta = 90°$.

a decrease in the electrolyte density. This lower density electrolyte is buoyed upward along the cathode if the cathode placement angle is $\Theta = 90°$. The flow goes out of the cavity along the upper sidewall of cavity. This outflow forms a large vortex above the cavity.[9] This mixes with the bulk electrolyte and the density becomes higher. The vortex collides with the lower end of the cathode and increases the current at the lower end of the cathode.

For the neighboring 200 μm cavities, the flow exiting the right cavity enters into the right end of the left side neighboring cavity (Fig. 4a). Since the cupric ion is already depleted on the right side cavity, flux of this entering flow into the left side cavity is smaller. Accordingly, the neighboring isoconcentration contours are closer at the right end of the right side cavity (Fig. 4b, arrow) than those at the right end of the left side cavity. The current becomes greater at the right end of the right side cavity (Fig. 4c, arrow).

Bump shapes for 100 and 50 μm cavities.—Figure 5 shows the cross section of bumps electrodeposited potentiostatically in the mass-transfer controlled region. The cathode widths are 100 and 50 μm and the aspect ratio is one for a and b, respectively. The cathode placement angles are $\Theta = 90°$.

For the 100 μm cathode width cavity of Fig. 5a, bump height increases toward right as was observed for the 200 μm cavities. For the 50 μm cavity of Fig. 5b, however, the bump height does not increase toward right and the shape is flat.

Numerical computation for 50 μm cavity.—Figure 6 shows the flow pattern, isoconcentration contour, and current distribution within the cavity of 50 μm cathode width of $\Theta = 90°$. A flow from the right side does not penetrate deep into the cavity (Fig. 6a). Figure 6b is the isoconcentration contour. The contours are parallel to the cathode and the cupric ion is transported mainly by the diffusion as opposed to convection.

Bump shapes for 30, 20, 10 μm cavities.—Figure 7 also shows the cross section of bumps at the mass-transfer controlled region. The cathode widths are 30, 20, and 10 μm and the aspect ratio is one for a, b, and c, respectively. The cathode placement angles are $\Theta = 90°$. The bump heights do not increase toward the right any more and their shapes are flat for these smaller cavities indicating that mass transport within these smaller cavities occurs by diffusion.

Conclusions

The electrodeposition into deep cavities with aspect ratio of one has been studied. The relative effects of natural convection *vs.* diffusion are discussed.

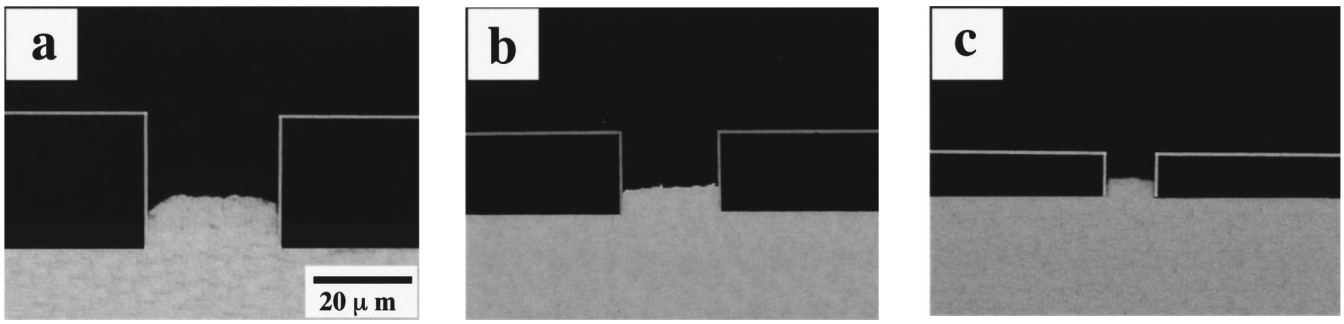

Figure 7. Cross section of bumps with different cathode widths; (a) 30, (b) 20, and (c) 10 μm.

1. The natural convection due to density difference is effective in stirring the inside of cavity with 200 μm width. The bump height increases toward lower side for cathode placement angle of $\Theta = 90°$. This increase in bump height results from a collision of flow along the lower side of the resist sidewall which enlarges local current and thickens the lower edge of bumps.

2. The natural convection also influences the bump height in neighboring cavities of 200 μm cathode width. The bump height becomes smaller for the upper side cavity compared to the lower side for neighboring cavities due to depletion effect.

3. The natural convection is not effective for cavities smaller than 100 μm in width. The bump shapes become flat as transport is controlled by diffusion within the cavities.

Acknowledgments

Part of the research was supported by Nissan Science Foundation, Japan.

Okayama University assisted in meeting the publication costs of this article.

List of Symbols

- c concentration, mol/m^3
- c_0 bulk concentration, mol/m^3
- D diffusion coefficient, m^2/s
- g gravitational force, m/s^2
- P pressure, kg/m s^2
- t time, s
- u velocity in x direction, m/s
- v velocity in y direction, m/s
- x x direction, m
- y y direction, m
- ρ density, kg/m^3
- β bulk expansion coefficient, m^3/mol
- μ viscosity, kg/s m
- ν kinematic viscosity, m/s

References

1. J. O. Dukovic, *IBM J. Res. Dev.*, **37**, 125 (1993).
2. K. Leyerdecker, W. Bacher, W. Stark, and A. Thopmmers, *Electrochim. Acta*, **39**, 1139 (1994).
3. K. Kondo, T. Miyazaki, and Y. Tamura, *J. Electrochem. Soc.*, **141**, 1644 (1994).
4. K. Kondo, K. Fukui, and K. Shinohara, *Kagaku Kogaku Ronbunshu*, **22**, 534 (1996).
5. K. Kondo, K. Fukui, K. Uno, and K. Shinohara, *J. Electrochem. Soc.*, **143**, 1880 (1996).
6. K. Kondo, K. Fukui, M. Yokoyama, and K. Shinohara, *J. Electrochem. Soc.*, **144**, 466 (1997).
7. K. Kondo and K. Fukui, *J. Electrochem. Soc.*, **145**, 840 (1998).
8. K. Kondo and K. Fukui, *J. Electrochem. Soc.*, **145**, 3007 (1998).
9. K. Fukui, M. Ayama, K. Hayashi, T. Yoneda, X. Tanaka, and K. Kondo, *J. Jpn. Inst. Electron. Packag.*, **2**, 35 (1999).